ACS APPLIED MATERIALS & INTERFACES

Research Article

www.acsami.org

Surface-Limited Synthesis of Pt Nanocluster Decorated Pd Hierarchical Structures with Enhanced Electrocatalytic Activity toward Oxygen Reduction Reaction

Tao Yang,*[,†] Guojian Cao,[‡] Qingli Huang,[§] Yanxia Ma,[†] Sheng Wan,[†] Hong Zhao,[†] Na Li,[†] Xia Sun,[†] and Fujun Yin[†]

[†]School of Chemical Engineering, Huaihai Institute of Technology, Lianyungang 222005, People's Republic of China

[‡]School of Materials Science and Engineering, Harbin University of Science and Technology, Harbin 150040, People's Republic of China

[§]Testing Center, Yangzhou University, Yangzhou, 225009, People's Republic of China

Supporting Information

ABSTRACT: Exploring superior catalysts with high catalytic activity and durability is of significant for the development of an electrochemical device involving the oxygen reduction reaction. This work describes the synthesis of Pt-on-Pd bimetallic heterogeneous nanostructures, and their high electrocatalytic activity toward the oxygen reduction reaction (ORR). Pt nanoclusters with a size of 1−2 nm were generated on Pd nanorods (NRs) through a modified Cu underpotential deposition (UPD) process free of potential control and a subsequent surface-limited redox reaction. The Pt nanocluster decorated Pd nanostructure with a ultralow Pt content of 1.5 wt % exhibited a mass activity of 105.3 mA mg^{-1} (Pt−Pd) toward ORR, comparable to that of the commercial Pt/C catalyst but 4 times higher than that of carbon supported Pd NRs. More importantly, the carbon supported Pt-on-Pd catalyst displays relatively small losses of 16% in electrochemical surface area (ECSA) and 32% in mass activity after 10 000 potential sweeps, in contrast to respective losses of 46 and 64% for the commercial Pt/C catalyst counterpart. The results demonstrated that Pt decoration might be an efficient way to improve the electrocatalytic activity of Pd and in turn allow Pd to be a promising substitution for commercial Pt catalyst.

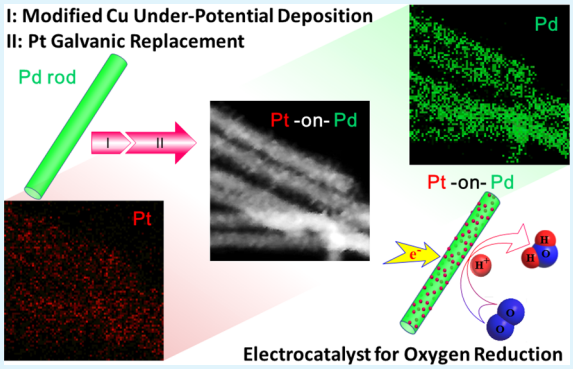

KEYWORDS: *electrocatalyst, heterogeneous nanostructure, oxygen reduction reaction, platinum, underpotential deposition*

INTRODUCTION

The development of highly efficient catalysts for the oxygen reduction reaction (ORR) is still challenging due to the complication of its kinetics process and the severity of the real application environment.[1,2] Multimetallic heterogeneous nanostructures have attracted increasing interest in a wide range of applications, especially in the catalytic field, such as organic catalysis,[3−5] photocatalysis,[6] and electrocatalysis.[7−9] Owing to the novel electronic and synergy effect at the well-defined multimetallic interface, such heterostructural catalysts usually outperform the counterpart alloys or monometallic components.[10−13] More recently, some noble metals such as Pt can obtain ultrahigh utilization at low loading amount by fabricating a Pt-rich skin/shell on heterogeneous catalysts,[14−17] especially quasi-one-dimensional nanostructures.[18−23] The lattice strain and adsorption behaviors of the surface Pt atoms would be greatly influenced by the core constituents,[24] resulting in the emergence of synergy effect.[25] Accordingly, most of the work was devoted to the influence of Pd core on the catalytic activity of Pt shell.[5,17,18,26−28] It is noteworthy that the catalysis of Pd toward ORR has been recognized and the activity has been greatly improved by alloying with transitional metals or tailoring the exposed facets.[29−34] However, little work has been dedicated to the variation of Pd catalysis affected by Pt shell, mainly because the previously reported Pt-on-Pd structures had very high Pt content and the surface was nearly completely covered by Pt. Another important issue about Pd catalysts is the inherent poor durability in acid solution associating with the low redox potential of Pd (0.915 V). If the catalytic activity and durability of Pd could be enhanced by Pt decoration with very low Pt content, it would open another avenue for expanding the real application of Pd catalysts.

Although different techniques, such as one-pot synthesis,[35] controlled galvanic replacement approach,[7] and seed-mediated growth,[36] have been applied to prepare such heterogeneous structures, there are still limitations originating from the

Received: May 10, 2015
Accepted: July 16, 2015
Published: July 16, 2015

DOI: 10.1021/acsami.5b04021
ACS Appl. Mater. Interfaces 2015, 7, 17162−17170

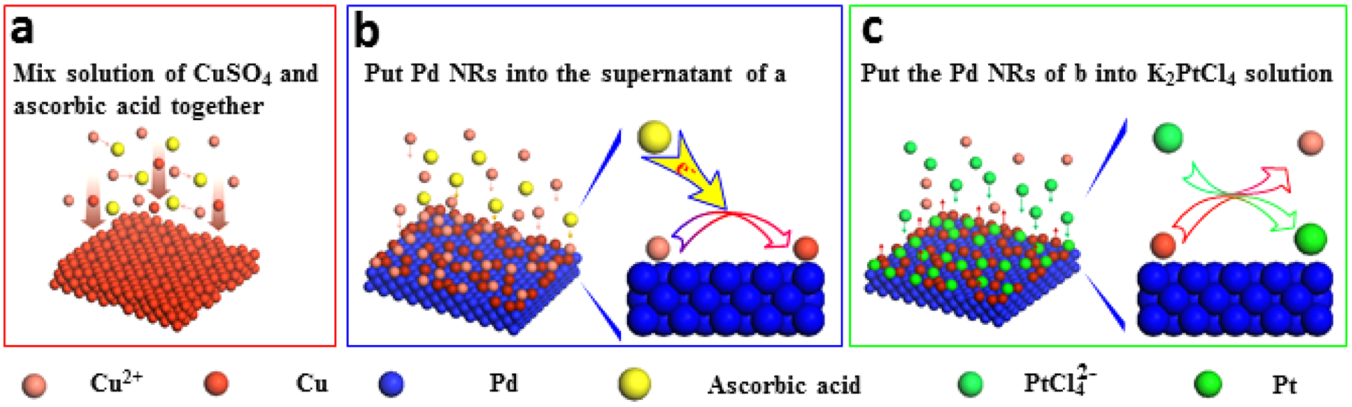

Figure 1. Illustration of the formation of Pt-on-Pt heterogeneous structure. (a) Cu^{2+} was reduced by ascorbic acid in the bulk solution. (b) Pd NRs were dispersed into the supernatant of (a), in which Cu^{2+} was reduced by ascorbic acid and deposited on Pd NR surface due to the UPD effect. (c) The Cu UPD layers were replaced by Pt via galvanic replacement reaction.

complex architectures or constituents. Therefore, developing a facile approach for producing nanoparticles with tailored heterostructures at the atomic level is always a challenge in nanoscience.[37]

Underpotential deposition (UPD) has been used to generate Pt catalytic monolayers for ORR, which involved a formation of Cu UPD layers due to the difference in work function and the subsequent surface-limited galvanic replacement reaction with Pt.[26,38,39] The value of UPD layers is a viability of atomic level control for the heterostructure. However, exterior power sources, functioning as electron providers and potential controllers, are necessary for the UPD process. Besides the use of exterior power sources, the core substrates should be supported on the conducting electrode to facilitate the electron flow from the exterior power sources to the adsorbed Cu^{2+}; therefore the final product is restricted to a relatively small amount.[40,41] The UPD effect has been used to direct the growth of some special nanocrystals with high index facets in seed-mediated approaches.[16,42−46] Generally, the concentration of the chemical reductants in the bulk solution was too low to reduce Ag^{+} or Cu^{2+}. However, the adsorbed Ag^{+} or Cu^{2+} on Au surface could be reduced at less negative redox potentials due to the larger difference in work function, e.g., UPD reduction.[47−49] In other words, Ag^{+} or Cu^{2+} could be reduced by chemical reductants with slightly lower concentrations.[16,45,46,50] All the work suggests the possibility of operating UPD in solution phase independent of exterior power sources.

Herein, we demonstrated a facile approach for fabricating a bimetallic heterogeneous structure consisting of ultrathin Pt nanoclusters on Pd nanorods (NRs) (Pt-on-Pd). The method involves generating Cu UPD layers on Pd NR surface and followed by surface-limited redox reaction (Figure 1). The Cu UPD layers were generated by reducing Cu^{2+} on Pd surface with L-ascorbic acid through a modified UPD process. Briefly, a solution was prepared in advance by mixing $CuSO_4$ with L-ascorbic acid at a higher concentration and leaving it undisturbed overnight (Figure 1a). Cupric ions were reduced by L-ascorbic acid gradually until the apparent redox reaction stopped. The supernatant was collected for the following use as UPD solution, in which the concentration of the remaining ascorbic acid was too low to reduce the rest of the cupric ions in the bulk solution. After dispersing Pd NRs into the UPD solution, similar to the case in seed-mediated growth of high index faceted Au−Pd alloys, the adsorbed Cu^{2+} on the Pd NR surface could be reduced by ascorbic acid due to the UPD effect (Figure 1b). The Cu UPD layers were finally replaced with Pt via the galvanic replacement process (Figure 1c).

In contrast to the conventional UPD process that involves exterior power sources and conducting support, Cu was UPD reduced by L-ascorbic acid in solution phase in the present approach, which can be potentially scaled to large production. Meanwhile, the termination of the surface redox reactions and the ultimate coverage of the UPD layer in the present modified UPD process will be very different from the previously produced heterostructures.[49,51,52] As an example for the present approach, a uniform Pt submonolayer was successfully built onto the Pd nanorods. Different from the previously reported Pt-on-Pd nanostructures, the present Pt submonolayer consisted of 1−2 nm nanoclusters with a very low content of 1.5 wt %. The superior catalytic performances of the Pt-on-Pd heterostructures were demonstrated by electrochemical catalyzing ORR and the durability test in $HClO_4$ solution.

EXPERIMENTAL SECTION

Synthesis of Pd Nanorods. Pd nanorods were prepared by a reported method with some modification.[53] Typically, palladium(II) chloride ($PdCl_2$, AR, Sinopharm Chemical Reagent Co. Ltd., 18.0 mg), polyvinylpyrrolidone (PVP, MW = 30 000, Sinopharm Chemical Reagent Co. Ltd., 800 mg), and sodium iodide (NaI, AR, Sinopharm Chemical Reagent Co. Ltd., 300 mg) were dispersed in 12.0 mL of deionized water. After forming a homogeneous dark red solution, the solution was sealed in a 25 mL Teflon-lined stainless-steel autoclave and then heated at 210 °C for 150 min. The products were finally precipitated with isopropanol and washed with ethanol at least five times.

Modified UPD for Cu layers on Pd NRs (Cu-on-Pd). Copper(II) sulfate pentahydrate ($CuSO_4·5H_2O$, AR, Sinopharm Chemical Reagent Co. Ltd., 250 mg) and L-ascorbic acid (AR, Sinopharm Chemical Reagent Co. Ltd., 264 mg) were dissolved in 50 mL of degassed deionized water, respectively. UPD solution was prepared by mixing these two solutions together in a 200 mL flask and sat undisturbed overnight at room temperature. During this time Cu was reduced and slowly precipitated at the flask bottom until the redox reactions between Cu^{2+} and ascorbic acid apparently stopped. A 10 mg sample of Pd NRs was then dispersed into 50 mL of the UPD supernatant and kept at room temperature for 3 h. Cu was deposited onto Pd NR surface with L-ascorbic acid at underpotential condition. The Cu-on-Pd nanoparticles were washed with degassed deionized water five times. UV−vis measurement was used to detect the existence of L-ascorbic acid in centrifugate solution. The UV−vis spectra in the wavelength range from 200 to 800 nm were detected,

DOI: 10.1021/acsami.5b04021
ACS Appl. Mater. Interfaces 2015, 7, 17162−17170

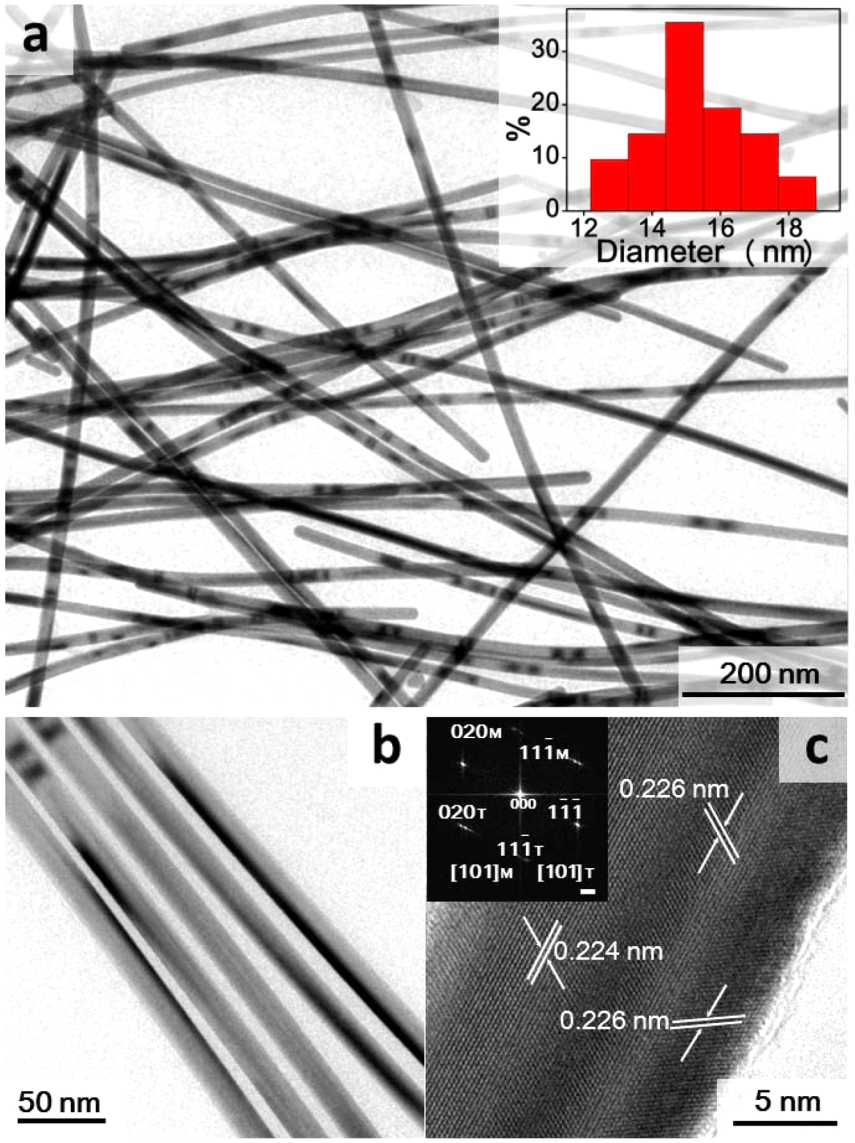

Figure 2. TEM and HRTEM images of Pd NRs. (a and b) TEM images of the as-made Pd NRs at different magnifications. (c) HRTEM image of the Pd rod. Inset of (a) is histogram for diameter distribution; inset of (c) is the corresponding FT pattern.

and the responses at 264 nm were used to compare the variation of L-ascorbic acid concentrations.

Formation of Pt Clusters on Pd NRs (Pt-on-Pd). The Cu-on-Pd nanoparticles were then dispersed into 50 mL of potassium chloroplatinite (K_2PtCl_4, AR, Aladdin Chemical Reagent Co. Ltd., 0.1 mM) for 30 min. The Cu UPD layers were replaced with Pt. The final product was washed with deionized water five times.

Structural Characterization. Transmission electron microscopy (TEM) and high-resolution transmission electron microscopy (HRTEM) micrographs of Pd NRs and bimetallic Pt-on-Pd particles were taken on a JEM-2100 TEM equipped with energy-dispersive X-ray analysis (EDXA). Powder X-ray diffraction (PXRD) of Pd NRs, Cu-on-Pd particles, and Pt-on-Pd particles were recorded on an X'Pert PRO MPD (Panalytical) system with a Cu Kα X-ray source (λ = 1.5405). Scanning transmission electron microscopy (STEM) micrographs of Pt-on-Pd were taken on a Tecnai G2 F30 S-TWIN, equipped with a high-angle annular dark-field (HAADF) detector. X-ray photoelectron spectroscopy (XPS) of Pt-on-Pd was performed on an ESCALAB 250Xi system; binding energies (BEs) were calibrated by setting the C 1s peak to 284.8 eV. The metal compositions were determined by a Bruker ICP-MS (M90) system. The catalyst loading amounts on carbon black were measured by thermogravimetric analysis (TGA) on a STA449F3 (METZSCH).

Preparation of Catalyst Ink and Working Electrode. To obtain carbon supported catalysts, a mixture solution of 5 mL of ethanol and 5 mL of chloroform consisting of 8 mg of carbon black (Cabot, Vulcan XC-72) and 2 mg of metallic catalysts (Pd NRs or Pt-on-Pd NRs) were ultrasonicated for 60 min and magnetically stirred for 3 h. The carbon supported catalysts were collected by centrifuge and dried for use. For homemade Nafion solution, 4 mL of deionized water, 1 mL of isopropanol, and 25 μL of Nafion (Sigma-Aldrich, 5 wt %) were mixed together and stirred to form a homogeneous solution. Then 5 mg of Pd NRs/C, Pt-on-Pd NRs/C, and commercial Pt/C (Johnson Matthey, 20 wt %) and 10 mg of commercial Pd/C (Sigma-Aldrich, 10 wt %) catalysts were dispersed into 5 mL of homemade Nafion solution, respectively. The working electrode was a glassy-carbon rotating disk electrode (RDE; Pine Instruments, 0.196 cm^2). A 20 μL volume of catalyst ink was dropped onto the working electrode with a pipet and dried in air flow; the metallic catalyst amount on the electrode was 4 μg.

Electrochemical Measurements. All the electrochemical measurements were carried out on an Autolab potentiostat/galvanostat (PGSTAT-302N) workstation in a three electrode cell at room temperature. A pure platinum foil with an area of 1.0 cm^2 was used as counter electrode. A saturated calomel electrode (SCE) in a separate compartment was used as reference. All the potentials in this paper

DOI: 10.1021/acsami.5b04021
ACS Appl. Mater. Interfaces 2015, 7, 17162−17170

were corrected to the reversible hydrogen electrode (RHE). Cyclic voltammetry (CV) curves were recorded in argon-saturated 0.1 M $HClO_4$ (Sinopharm Chemical Reagent Co. Ltd.) in the potential range of 0.05−1.2 V with a sweep rate of 50 mV s^{-1}. Before each test, the electrode was pretreated by carrying out CV until a stable curve was obtained. CO stripping was performed as the following procedure: In an argon-saturated 0.1 M $HClO_4$ solution, the working electrode was maintained at 0.05 V for 40 min, during which CO was bubbled in the first 20 min to absorb CO on the catalyst surface; argon was then bubbled in the remaining 20 min to drive CO out of the solution completely; a linear potential scan was then carried out from 0.4 to 1.2 V at a sweep rate of 50 mV s^{-1} with argon bubbling. ORR polarization curves were recorded in oxygen-saturated 0.1 M $HClO_4$ solution from 0 to 1.1 V with a sweep rate of 10 mV s^{-1} and a rotation rate of 1600 rpm. The accelerated durability test (ADT) was performed in the CV pattern from 0.6 to 1.1 V for 10 000 cycles with a sweep rate of 50 mV s^{-1} in oxygen-saturated 0.1 M $HClO_4$ solution.

The electrochemical surface area (ECSA) was evaluated by integrating the charge associated with the CO stripping. The electrooxidation of CO_{ad} monolayer on the catalyst surface was assumed to be 420 μC cm^{-2}.[54,55]

The specific activity (i_a) and mass activity (i_m) for ORR were calculated based on the ORR polarization curves. The kinetic current (i_k) can be calculated by the Koutecky−Levich equation:

$$1/i = 1/i_d + 1/i_k \quad (1)$$

where i_d is the diffusion-limiting current.

$$i_m = i_k/m \quad (2)$$

$$i_a = i_m/\mathrm{ECSA} \quad (3)$$

RESULTS AND DISCUSSION

Structure Characterization. Pd NRs were prepared via the reduction of $PdCl_2$ with PVP in the presence of NaI.[53] Transmission electron microscopy (TEM) images of the product at different magnifications are shown in Figure 2. Figure 2a displays an overview of the product, which consists of uniform nanostructures with rod shapes. The nanorods (NRs) have an average diameter of 15 nm (inset of Figure 2a) and lengths in the micrometer range up to 3 μm (see the Supporting Information, Figure S1). The HRTEM image (Figure 2b) demonstrates that the Pd rods have a smooth surface and uniform diameter along the rods. The planes with interplanar spacings of 0.226 and 0.224 nm shown in Figure 2c are highly consistent with the (111) plane of the Pd NR surface structure.[56] The corresponding Fourier transform (FT) pattern reveals that the produced Pd NRs are twinned structure (inset of Figure 2c), which was also evidenced by the selected area electron diffraction (SAED) characterization results (Supporting Information, Figure S2).[56]

Pt-on-Pd bimetallic heterostructure was fabricated on the Pd NRs through the present modified Cu UPD and the subsequent galvanic replacement reaction (see the Experimental Section for details). TEM was applied to study the structures and crystallization of the formed materials. Typical TEM images (Figure 3a,b) demonstrate that a number of small clusters had grown onto the Pd NRs at multiple sites evidenced as the dark points. The clusters are 1−2 nm in size with irregular shape. Based on energy-dispersive X-ray spectroscopy (EDS) analysis, the small clusters were determined to be Pt (inset of Figure 3a). The Cu signal was mainly from the TEM grid. High-resolution TEM (HRTEM) images of the circled regions in Figure 3b show some concave−convex edges due to the growth of Pt clusters (Figure 3c,d). In comparison with Pd(111) with an interplanar spacing of 0.226 nm, a slightly

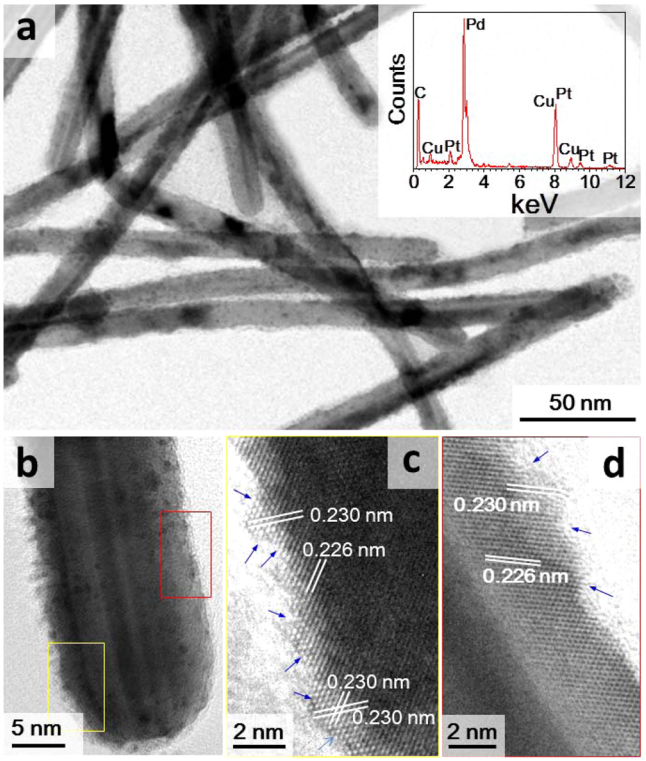

Figure 3. TEM and HRTEM images of Pt-on-Pd NRs. (a) TEM image of Pt-on-Pd NRs. (b) HRTEM image of the tip region of one Pt-on-Pd rod. (c) and (d) are the enlarged images of the circled regions of (b). Inset of (a) is the TEM−EDS spectrum of Pt-on-Pd NRs.

larger interplanar spacing of 0.230 nm could be assigned to the Pt(111) surface.[57] The lattice fringes coherently extended from the body of Pd rod to the convex clusters, implying the epitaxial growth of Pt clusters with a very high degree of crystallinity. The epitaxial growth has been reported in conventional UPD method,[51,58] which might provide extra stability against Pt nanoparticles' ripening and aggregation. Additionally, the epitaxial growth of Pt on Pd might form compressive strain due to the lattice mismatch, which was demonstrated to weaken the adsorption of oxygenated species, resulting in enhanced catalytic performance toward ORR.[26,28,59] It should be noted that the Pt-on-Pd surface is quite rough and many atomic steps are exposed as indicated by the arrows in Figure 3c,d. These open surface atomic arrangements have demonstrated high catalytic activity.[5]

Dispersion of Pt clusters was further characterized by high-angle annular dark-field (HAADF) STEM. The images in Figure 4 show the intense bright contrast near the surface, indicating the existence of a heavier element, i.e., Pt (Z = 78) on the Pd (Z = 46) NR surface. The Pt clusters are highly dispersed over the entire surface of the Pd NRs with an approximate size of ∼2 nm, which is consistent with the HRTEM results. The EDS mapping in Figure 4b also shows the Pt and Pd distribution on the bimetallic heterostructure. Both TEM and STEM analyses confirmed the formation of Pt clusters on Pd NR surface. Because of the strong surface energy, Pt preferentially formed stable structures such as clusters or island on the core substrates,[5,6] which might possess more durability in applications. The overall weight percentage of Pt in our Pt-on-Pd structure is as low as 1.5%, which was

DOI: 10.1021/acsami.5b04021
ACS Appl. Mater. Interfaces 2015, 7, 17162−17170

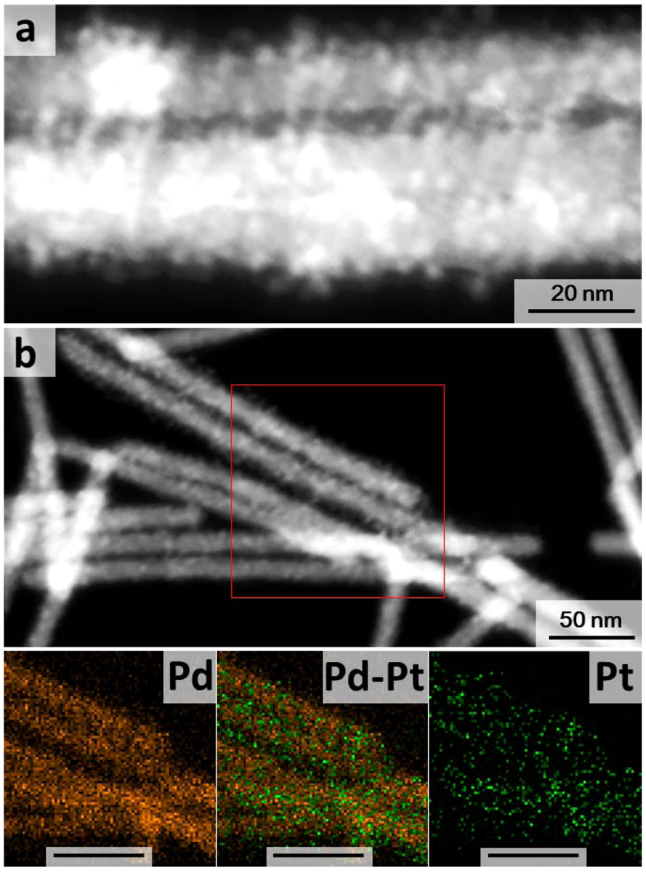

Figure 4. STEM images and EDS mappings of Pt-on-Pd heterostructure. (a) STEM image of Pt-on-Pd NRs. (b) STEM image and corresponding EDS mappings of Pd and Pt. The scale bars in EDS mappings are 20 nm.

determined by inductively coupled plasma mass spectrometry (ICP-MS) measurements. To the best of our knowledge, this is the lowest Pt content ever reported in this kind of Pt-on-Pd heterogeneous catalyst.[21,25,57]

It should be note that our Pt-on-Pd heterostructure is very different from the reported either Pt monolayer or Pt dendrites on Pd cores. Most of the reported nanostructures had high Pt content and nearly fully covered Pt surface.[5,17,18,21−23,57,60] In contrast, the present Pt-on-Pd structure has ultralow Pt content and most of the Pd surface is still exposed. Thus, the present heterogeneous structure should be better described as Pt nanocluster decorated Pd NRs.

The formation and sacrifice of Cu UPD layers was verified by X-ray diffraction (XRD) characterizations. In XRD spectra, the weak peaks at 36.5, 43.5, 50.6, and 73.8° indicate the existence of Cu on Pd NRs after the modified UPD process (Supporting Information, Figure S3). While no peaks can be indexed to Cu in Pt-on-Pd XRD spectra, this implies that most Cu constituents were replaced by Pt. There must be cuprous oxide or copper oxide formed in the sacrificial Cu layer because of the exposure in air. The possible remaining copper oxide in Pt-on-Pd that cannot be detected by XRD might be due to the ultralow content or the poor crystallization, which can be determined by an XPS test. Figure S4a in the Supporting Information shows the overview X-ray photoelectron spectroscopy (XPS) spectra of Pt-on-Pd; the peaks of Pd, Pt, and Cu can be observed clearly. Figure S4b,c in the Supporting Information shows the high resolution scans of Pd 3d and Pt 4f verifying the presence of Pt on Pd surface. The energy binding peak at 932.28 eV can be assigned to Cu $2p_{3/2}$ (Supporting Information, Figure S4d).[50]

It is noted that the Cu UPD treatment is essential for the formation of Pt clusters. No Pt clusters formed on the Pd NRs without involving $CuSO_4$ in the preparation procedure (Supporting Information, Figure S5). Isolated Pt nanoparticles were produced by dispersing Pd NRs into the solution with low concentrations of K_2PtCl_4 and ascorbic acid (Supporting Information, Figure S6).

In distinction to conventional UPD process, the modified UPD is free of exterior power sources and in favor of large scale. In addition, complete Pt-on-Pd nanoparticles can be obtained because conducting support is not necessary.

Electrochemical Performance. Electrocatalytic properties of the Pt-on-Pd were benchmarked toward ORR against commercial Pt/C catalyst. Cyclic voltammetry (CV) tests can provide powerful information on the surface compositions and structures. Figure 5a shows CV curves of Pt-on-Pd/C, Pd NRs/C, commercial Pt/C, and Pd/C catalysts. All the samples containing Pd exhibit two distinct peaks associated with H_{upd} adsorption (<0.4 V) and $Pd(OH)_2$ reduction (>0.6 V) in the cathodic scan. In comparison with Pd/C and Pd NRs/C, Pt-on-Pd/C shifted its $Pd(OH)_2$ reduction peak to a slightly higher potential due to the covering of Pt clusters. Moreover, in comparison with Pd NRs/C, Pt-on-Pd/C presents more reversible H_{upd} adsorption/desorption peaks at ∼0.05 V, suggesting the existence of ordered Pt surface structures.[27] CO stripping behavior was determined by comparing the first and second linear voltammetry curves (Figure 5b). Compared with Pd NRs/C, Pt-on-Pd/C displayed a negative shift in the CO peaks. All the results are highly consistent with the reported properties of Pt-on-Pd nanostructure.[27] These characteristic peaks of Pt-on-Pd/C are still different from those of Pt/C catalyst, which might be due to the ultralow Pt

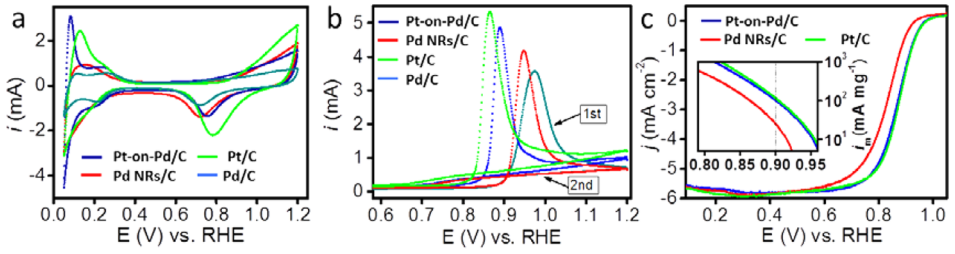

Figure 5. Electrochemical measurements results. (a and b) CV and CO stripping curves of Pt-on-Pd/C, Pd NRs/C, commercial Pt/C, and Pd/C catalysts. The current (i) was magnified 10 times to be shown clearly. (c) ORR polarization curves of Pt-on-Pd/C, Pd NRs/C, and commercial Pt/C. The inset is the mass activities comparison.

DOI: 10.1021/acsami.5b04021
ACS Appl. Mater. Interfaces 2015, 7, 17162−17170

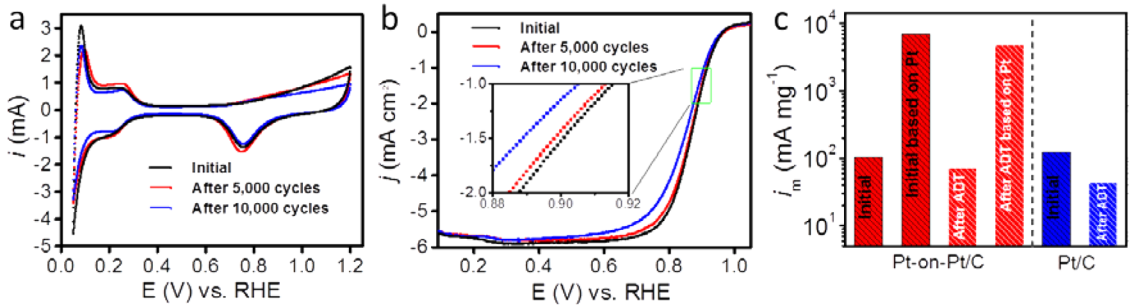

Figure 6. Duration test results. (a and b) CV and ORR polarization curves of Pt-on-Pd/C catalyst at different stages in duration test. (c) Comparison of Pt-on-Pd/C and Pt/C in terms of mass activity.

content and the still exposed Pd surface. Before each electrochemical measurement, a pretreatment of CV cycling was performed until stable CV curves were obtained. The reported nanowires with Pt shell/skin and their ECSAs are compared in Table S1 in the Supporting Information. Pt-on-Pd/C (57.5 m^2 g^{-1}) displayed 14.3% higher ECSA than that of Pd NRs/C (50.3 m^2 g^{-1}) due to the formation of Pt clusters. Note that ECSA of Pt-on-Pd/C is still smaller than that of Pt/C (64.8 m^2 g^{-1}), perhaps due to their relatively large overall particle size (Supporting Information, Table S2).

The ORR polarization curves of Pd NRs/C, Pt-on-Pd/C, and commercial Pt/C are shown in Figure 5c. All the catalysts displayed two distinct regions of diffusion-limiting (below 0.6 V) and mixed kinetic diffusion (0.6−1.0 V). The polarization curve of Pt-on-Pd/C was very close to that of Pt/C. Pt-on-Pd/C had a half-wave potential ($E_{1/2}$) of 0.862 V, which was very comparable to that of Pt/C (0.868 V) and much higher than that of Pd NRs/C (0.823 V). The kinetic current densities at 0.9 V were calculated by correcting the mass transport according to the Levich−Koutecky equation, and normalized with respect to both ECSA and the loading amount of metallic catalysts (Supporting Information, Table S2). Pt-on-Pd/C (0.183 mA cm^{-2}) displayed a specific activity (i_a) nearly 4 times that of Pd NRs/C (0.052 mA cm^{-2}) and comparable to that of Pt/C (0.188 mA cm^{-2}). Pt-on-Pd/C also showed a high mass activity of 105.3 mA mg^{-1}, which was 85.6% that of Pt/C (122.00 mA mg^{-1}) and 4 times greater than that of Pd NRs/C (26.19 mA mg^{-1}) (Figure 5c). Pt-on-Pd/C shows comparable to but slightly lower activity than that of Pt/C in terms of specific and mass activities. The previously reported Pt-on-Pd heterogeneous nanostructures presented much higher catalytic activity over Pt/C catalyst mainly due to the high Pt content, and the catalytic performances of Pt were enhanced by the cooperation with Pd.[5,21,26] While the present Pt-on-Pd catalyst is Pt decorated Pd catalyst with ultralow Pt content, the main catalytic activity still comes from the Pd surface.

If the Pt nanoclusters on the Pd NRs/C were solely taken into account, Pt-on-Pd/C (7010 mA mg_{Pt}^{-1}) exhibited an extraordinary improvement factor of 57 versus commercial Pt/C catalyst (Supporting Information, Table S2). This high performance has not been reported, though the ultrahigh catalytic performance of Pt nanoclusters has been demonstrated.[24,61] Meanwhile, considering the low Pt coverage (see TEM and STEM analysis) and the ultralow Pt content (1.5 wt %), the exposed Pd surface must also contribute to the electrocatalysis. If we simply add the activities of Pt and Pd together, the mass activity (122·1.5% + 26.19(1 − 1.5%) = 27.62 mA mg^{-1}) is much lower than that of Pt-on-Pd/C (105.3 mA mg^{-1}). According to the above discussion, the catalytic performance of Pt-on-Pd/C is more rational to be originated from the Pd catalytic surface enhanced by the decoration of Pt clusters. Thus, the catalytic surface is very different from the Pt monolayer or the thick Pt shell.[5,9,21,26,60]

Accelerated durability test (ADT) was performed for 10 000 cycles. After 5000 cycles, the CV and ORR polarization curves show no obvious change in comparison with the initial CV and ORR curves (Figure 6a). After cycling for up to 10 000 cycles, Pt-on-Pd/C only lost 16% of the initial ECSA value, while in a vast contrast Pt/C displayed a loss of 45.6% because of the dissolution of Pt surface atoms and agglomeration of Pt particles through surface oxidation/reduction processes (Supporting Information, Figure S7, Table S2).[62−64] Pt-on-Pd/C displays only about 19 and 32% losses of initial i_a and i_m values (Figure 6c, Table S2 in the Supporting Information). However, the commercial Pt/C catalyst degraded badly: about 34% for i_a and 64% for i_m (Supporting Information, Figure S8, Table S2). It should be noted that the degradation of catalyst is highly related to the experimental details. In comparison with the present work, the commercial TKK Pt/C catalyst previously displayed smaller losses in ECSA and mass activity after a different durability test, which included 7200 sweeps of potential cycling from 0.6 to 1.0 V in a rectangular wave pattern.[2] No obvious change can be observed from TEM images of carbon supported Pt-on-Pd and Pd NRs catalysts before and after duration cycling (Supporting Information, Figures S9−S11). The rapid deterioration of Pt/C is perhaps caused by Pt nanoparticles' ripening and aggregation (Supporting Information, Figure S12).[2] The above results evidently revealed the better durability of Pt-on-Pd, perhaps thanks to the epitaxial growth of Pt on Pd surface, which provide enhanced stability against ripening and aggregation.[5,57]

CONCLUSION

In summary, we reported a modified UPD approach for synthesizing heterostructural Pt-on-Pd electrocatalyst featuring highly distributed Pt nanoclusters covering Pd NRs. This approach takes place in an aqueous phase free of potential control and conducting support, which differentiates it from the conventional UPD method. The Pt-on-Pd catalyst exhibits excellent electrocatalytic performance. A typical example, the Pt-on-Pd catalyst displayed a mass activity as high as 105.3 mA mg^{-1} at 0.9 V for ORR with a Pt content as low as 1.5 wt %. In addition to the high intrinsic mass activity, the present Pt-on-Pd catalyst showed remarkable durability in acid media. These electrochemical results demonstrate that the reported hierarchical Pt-on-Pd is a desirable substitution for Pt with low cost toward ORR. The decoration of Pt nanoclusters might also be expanded to enhance the catalytic activity of Pd(110) and

DOI: 10.1021/acsami.5b04021
ACS Appl. Mater. Interfaces 2015, 7, 17162−17170

Pd(100) surfaces, which show intrinsically higher catalysis than that of Pd(111).[29,30,32,65] The method reported here also shows the potential in scalable production of bimetallic or multimetallic heterostructures with unique surface atomic arrangement and electronic properties resulting in enhanced catalytic performance.

■ ASSOCIATED CONTENT

Supporting Information

TEM, HRTEM, and SAED of the as-made Pd RNs, XRD pattern and XPS spectra of Pt-on-Pd, TEM and HRTEM of Pd NRs that underwent the two-step procedure without involving $CuSO_4$, TEM of the product by putting Pd NRs into the mixed solution of ascorbic acid and K_2PtCl_4, CV and ORR polarization curves of Pd NRs during the ADT measurement, TEM of the carbon supported Pt-on-Pd, Pd NRs and the commercial Pt/C catalysts before and after ADT measurement, comparison of electrochemical active surface area (EASA) with the reported nanowires, the variation of mass activity, specific activity, and EASA of Pt-on-Pd, Pd NRs, and the commercial Pt/C catalysts after ADT measurement. The Supporting Information is available free of charge on the ACS Publications website at DOI: 10.1021/acsami.5b04021.

■ AUTHOR INFORMATION

Corresponding Author

*E-mail: yangtao_hit@163.com.

Notes

The authors declare no competing financial interest.

■ ACKNOWLEDGMENTS

This work was supported by the National Natural Science Foundation of China (NSFC, No. 21473067) and the Scientific and Technological Program of Lianyungang (No. CG1307). We thank Chuanqiang Zhou at Yangzhou University for XPS measurements and Jiangsu Mariner Resources Development Research Institute for XRD, TGA, and ICP measurements.

■ REFERENCES

(1) Gasteiger, H. A.; Kocha, S. S.; Sompalli, B.; Wagner, F. T. Activity Benchmarks and Requirements for Pt, Pt-Alloy, and Non-Pt Oxygen Reduction Catalysts for PEMFCs. *Appl. Catal., B* **2005**, *56* (1−2), 9−35.

(2) Takahashi, I.; Kocha, S. S. Examination of the Activity and Durability of PEMFC Catalysts in Liquid Electrolytes. *J. Power Sources* **2010**, *195*, 6312−6322.

(3) Serpell, C. J.; Cookson, J.; Ozkaya, D.; Beer, P. D. Core@Shell Bimetallic Nanoparticle Synthesis via Anion Coordination. *Nat. Chem.* **2011**, *3* (6), 478−483.

(4) Chng, L. L.; Erathodiyil, N.; Ying, J. Y. Nanostructured Catalysts for Organic Transformations. *Acc. Chem. Res.* **2013**, *46* (8), 1825−1837.

(5) Lim, B.; Jiang, M. J.; Camargo, P. H. C.; Cho, E. C.; Tao, J.; Lu, X. M.; Zhu, Y. M.; Xia, Y. N. Pd-Pt Bimetallic Nanodendrites with High Activity for Oxygen Reduction. *Science* **2009**, *324*, 1302−1304.

(6) Dasgupta, N. P.; Liu, C.; Andrews, S.; Prinz, F. B.; Yang, P. Atomic Layer Deposition of Platinum Catalysts on Nanowire Surfaces for Photoelectrochemical Water Reduction. *J. Am. Chem. Soc.* **2013**, *135* (35), 12932−12935.

(7) Chen, C.; Kang, Y.; Huo, Z.; Zhu, Z.; Huang, W.; Xin, H. L.; Snyder, J. D.; Li, D.; Herron, J. A.; Mavrikakis, M.; Chi, M.; More, K. L.; Li, Y.; Markovic, N. M.; Somorjai, G. A.; Yang, P.; Stamenkovic, V. R. Highly Crystalline Multimetallic Nanoframes with Three-Dimensional Electrocatalytic Surfaces. *Science* **2014**, *343*, 1339−1343.

(8) Wu, Y.; Wang, D.; Chen, X.; Zhou, G.; Yu, R.; Li, Y. Defect-Dominated Shape Recovery of Nanocrystals: A New Strategy for Trimetallic Catalysts. *J. Am. Chem. Soc.* **2013**, *135*, 12220−12223.

(9) Zhang, J.; Sasaki, K.; Sutter, E.; Adzic, R. R. Stabilization of Platinum Oxygen-Reduction Electrocatalysts Using Gold Clusters. *Science* **2007**, *315*, 220−222.

(10) Erikson, H.; Sarapuu, A.; Alexeyeva, N.; Tammeveski, K.; Solla-Gullón, J.; Feliu, J. M. Electrochemical Reduction of Oxygen on Palladium Nanocubes in Acid and Alkaline Solutions. *Electrochim. Acta* **2012**, *59* (0), 329−335.

(11) Moghimi, N.; Abdellah, M.; Thomas, J. P.; Mohapatra, M.; Leung, K. T. Bimetallic FeNi Concave Nanocubes and Nanocages. *J. Am. Chem. Soc.* **2013**, *135* (30), 10958−10961.

(12) Huang, X.; Li, Y.; Zhou, H.; Zhong, X.; Duan, X.; Huang, Y. Simplifying the Creation of Dumbbell-Like Cu-Ag Nanostructures and Their Enhanced Catalytic Activity. *Chem. - Eur. J.* **2012**, *18* (31), 9505−9510.

(13) Goodman, A. M.; Cao, Y.; Urban, C.; Neumann, O.; Ayala-Orozco, C.; Knight, M. W.; Joshi, A.; Nordlander, P.; Halas, N. J. The Surprising in Vivo Instability of Near-IR-Absorbing Hollow Au−Ag Nanoshells. *ACS Nano* **2014**, *8* (4), 3222−3231.

(14) Wang, G.; Huang, B.; Xiao, L.; Ren, Z.; Chen, H.; Wang, D.; Abruña, H. D.; Lu, J.; Zhuang, L. Pt Skin on AuCu Intermetallic Substrate: A Strategy to Maximize Pt Utilization for Fuel Cells. *J. Am. Chem. Soc.* **2014**, *136* (27), 9643−9649.

(15) Sun, X.; Li, D.; Ding, Y.; Zhu, W.; Guo, S.; Wang, Z. L.; Sun, S. Core/Shell Au/CuPt Nanoparticles and Their Dual Electrocatalysis for Both Reduction and Oxidation Reactions. *J. Am. Chem. Soc.* **2014**, *136* (15), 5745−5749.

(16) Mazumder, V.; Chi, M.; More, K. L.; Sun, S. Core/Shell Pd/FePt Nanoparticles as an Active and Durable Catalyst for the Oxygen Reduction Reaction. *J. Am. Chem. Soc.* **2010**, *132* (23), 7848−7849.

(17) Sasaki, K.; Naohara, H.; Cai, Y.; Choi, Y. M.; Liu, P.; Vukmirovic, M. B.; Wang, J. X.; Adzic, R. R. Core-Protected Platinum Monolayer Shell High-Stability Electrocatalysts for Fuel-Cell Cathodes. *Angew. Chem., Int. Ed.* **2010**, *49* (46), 8602−8607.

(18) Koenigsmann, C.; Santulli, A. C.; Gong, K.; Vukmirovic, M. B.; Zhou, W.-p.; Sutter, E.; Wong, S. S.; Adzic, R. R. Enhanced Electrocatalytic Performance of Processed, Ultrathin, Supported Pd−Pt Core−Shell Nanowire Catalysts for the Oxygen Reduction Reaction. *J. Am. Chem. Soc.* **2011**, *133* (25), 9783−9795.

(19) Alia, S. M.; Pivovar, B. S.; Yan, Y. Platinum-Coated Copper Nanowires with High Activity for Hydrogen Oxidation Reaction in Base. *J. Am. Chem. Soc.* **2013**, *135* (36), 13473−13478.

(20) Guo, S.; Zhang, S.; Su, D.; Sun, S. Seed-Mediated Synthesis of Core/Shell FePtM/FePt (M = Pd, Au) Nanowires and Their Electrocatalysis for Oxygen Reduction Reaction. *J. Am. Chem. Soc.* **2013**, *135* (37), 13879−84.

(21) Guo, S.; Dong, S.; Wang, E. Ultralong Pt-on-Pd Bimetallic Nanowires with Nanoporous Surface: Nanodendritic Structure for Enhanced Electrocatalytic Activity. *Chem. Commun.* **2010**, *46*, 1869−1871.

(22) Bliznakov, S. T.; Vukmirovic, M. B.; Yang, L.; Sutter, E. A.; Adzic, R. R. Pt Monolayer on Electrodeposited Pd Nanostructures: Advanced Cathode Catalysts for PEM Fuel Cells. *J. Electrochem. Soc.* **2012**, *159* (9), F501−F506.

(23) Koenigsmann, C.; Sutter, E.; Chiesa, T. A.; Adzic, R. R.; Wong, S. S. Highly Enhanced Electrocatalytic Oxygen Reduction Performance Observed in Bimetallic Palladium-Based Nanowires Prepared under Ambient, Surfactantless Conditions. *Nano Lett.* **2012**, *12*, 2013−2020.

(24) Tiwari, J. N.; Nath, K.; Kumar, S.; Tiwari, R. N.; Kemp, K. C.; Le, N. H.; Youn, D. H.; Lee, J. S.; Kim, K. S. Stable Platinum Nanoclusters on Genomic DNA−Graphene Oxide with a High Oxygen Reduction Reaction Activity. *Nat. Commun.* **2013**, *4*, 1−7.

(25) Zhang, H.; Jin, M.; Xia, Y. Enhancing the Catalytic and Electrocatalytic Properties of Pt-Based Catalysts by Forming Bimetallic Nanocrystals with Pd. *Chem. Soc. Rev.* **2012**, *41* (24), 8035−8049.

(26) Adzic, R. R.; Zhang, J.; Sasaki, K.; Vukmirovic, M. B.; Shao, M.; Wang, J. X.; Nilekar, A. U.; Mavrikakis, M.; Valerio, J. A.; Uribe, F.

DOI: 10.1021/acsami.5b04021
ACS Appl. Mater. Interfaces 2015, 7, 17162−17170

Platinum Monolayer Fuel Cell Electrocatalysts. *Top. Catal.* **2007**, *46* (3−4), 249−262.
(27) Wells, P. P.; Crabb, E. M.; King, C. R.; Wiltshire, R.; Billsborrow, B.; Thompsett, D.; Russell, A. E. Preparation, Structure, and Stability of Pt and Pd Monolayer Modified Pd and Pt Electrocatalysts. *Phys. Chem. Chem. Phys.* **2009**, *11* (27), 5773−5781.
(28) Zhang, J.; Mo, Y.; Vukmirovic, M. B.; Klie, R.; Sasaki, K.; Adzic, R. R. Platinum Monolayer Electrocatalysts for O_2 Reduction: Pt Monolayer on Pd(111) and on Carbon-Supported Pd Nanoparticles. *J. Phys. Chem. B* **2004**, *108*, 10955−10964.
(29) Kondo, S.; Nakamura, M.; Maki, N.; Hoshi, N. Active Sites for the Oxygen Reduction Reaction on the Low and High Index Planes of Palladium. *J. Phys. Chem. C* **2009**, *113* (29), 12625−12628.
(30) Xiao, L.; Zhuang, L.; Liu, Y.; Lu, J.; Abruña, H. c. D. Activating Pd by Morphology Tailoring for Oxygen Reduction. *J. Am. Chem. Soc.* **2009**, *131* (2), 602−608.
(31) Shao, M.-H.; Sasaki, K.; Adzic, R. R. Pd−Fe Nanoparticles as Electrocatalysts for Oxygen Reduction. *J. Am. Chem. Soc.* **2006**, *128* (11), 3526−3527.
(32) Shao, M.; Yu, T.; Odell, J. H.; Jin, M.; Xia, Y. Structural Dependence of Oxygen Reduction Reaction on Palladium Nanocrystals. *Chem. Commun.* **2011**, *47* (23), 6566−6568.
(33) Yang, X.; Hu, J.; Fu, J.; Wu, R.; Koel, B. E. Role of Surface Iron in Enhanced Activity for the Oxygen Reduction Reaction on a $Pd_3Fe(111)$ Single-Crystal Alloy. *Angew. Chem., Int. Ed.* **2011**, *50* (43), 10182−10185.
(34) Kariuki, N. N.; Wang, X.; Mawdsley, J. R.; Ferrandon, M. S.; Niyogi, S. G.; Vaughey, J. T.; Myers, D. J. Colloidal Synthesis and Characterization of Carbon-Supported Pd−Cu Nanoparticle Oxygen Reduction Electrocatalysts. *Chem. Mater.* **2010**, *22* (14), 4144−4152.
(35) Li, C.; Sun, L.; Sun, Y.; Teranishi, T. One-Pot Controllable Synthesis of Au@Ag Heterogeneous Nanorods with Highly Tunable Plasmonic Absorption. *Chem. Mater.* **2013**, *25* (13), 2580−2590.
(36) Habas, S. E.; Lee, H.; Radmilovic, V.; Somorjai, G. A.; Yang, P. Shaping Binary Metal Nanocrystals through Epitaxial Seeded Growth. *Nat. Mater.* **2007**, *6*, 692−697.
(37) González, E.; Arbiol, J.; Puntes, V. F. Carving at the Nanoscale: Sequential Galvanic Exchange and Kirkendall Growth at Room Temperature. *Science* **2011**, *334* (6061), 1377−1380.
(38) Gokcen, D.; Bae, S.-E.; Brankovic, S. R. Stoichiometry of Pt Submonolayer Deposition via Surface-Limited Redox Replacement Reaction. *J. Electrochem. Soc.* **2010**, *157* (11), D582−D587.
(39) Kim, Y.-G.; Kim, J. Y.; Vairavapandian, D.; Stickney, J. L. Platinum Nanofilm Formation by EC-ALE via Redox Replacement of UPD Copper: Studies Using in-Situ Scanning Tunneling Microscopy. *J. Phys. Chem. B* **2006**, *110* (36), 17998−18006.
(40) Fonticelli, M. H.; Corthey, G. n.; Benitez, G. A.; Salvarezza, R. C.; Giovanetti, L. J.; Requejo, F. l. G.; Shon, Y. S. Preparation of Ultrathin Thiolate-Covered Bimetallic Systems: From Extended Planar to Nanoparticle Surfaces. *J. Phys. Chem. C* **2007**, *111*, 9359−9364.
(41) Park, S.; Yang, P.; Corredor, P.; Weaver, M. J. Transition Metal-Coated Nanoparticle Films: Vibrational Characterization with Surface-Enhanced Raman Scattering. *J. Am. Chem. Soc.* **2002**, *124* (11), 2428−2429.
(42) Seo, D.; Park, J. C.; Song, H. Polyhedral Gold Nanocrystals with O_h Symmetry: From Octahedra to Cubes. *J. Am. Chem. Soc.* **2006**, *128* (46), 14863−14870.
(43) Kim, F.; Song, J. H.; Yang, P. Photochemical Synthesis of Gold Nanorods. *J. Am. Chem. Soc.* **2002**, *124* (48), 14316−14317.
(44) Grzelczak, M.; Perez-Juste, J.; Mulvaney, P.; Liz-Marzan, L. M. Shape Control in Gold Nanoparticle Synthesis. *Chem. Soc. Rev.* **2008**, *37* (9), 1783−1791.
(45) Liu, M.; Guyot-Sionnest, P. Mechanism of Silver(I)-Assisted Growth of Gold Nanorods and Bipyramids. *J. Phys. Chem. B* **2005**, *109*, 22192−22200.
(46) Seo, D.; Yoo, C. I.; Park, J. C.; Park, S. M.; Ryu, S.; Song, H. Directed Surface Overgrowth and Morphology Control of Polyhedral Gold Nanocrystals. *Angew. Chem., Int. Ed.* **2008**, *47* (4), 763−467.
(47) Michaelson, H. B. Relation between an Atomic Electronegativity Scale and the Work Function. *IBM J. Res. Dev.* **1978**, *22* (1), 72−80.
(48) Rogers, L. B.; Krause, D. P.; Griess, J. C.; Ehrlinger, D. B. The Electrodeposition Behavior of Traces of Silver. *J. Electrochem. Soc.* **1949**, *95*, 33−46.
(49) Gokcen, D.; Bae, S.-E.; Brankovic, S. R. Reaction Kinetics of Metal Deposition via Surface Limited Red-Ox Replacement of Under Potentially Deposited Metal Monolayers. *Electrochim. Acta* **2011**, *56*, 5545−5553.
(50) Zhang, L.; Zhang, J.; Kuang, Q.; Xie, S.; Jiang, Z.; Xie, Z.; Zheng, L. Cu^{2+}-Assisted Synthesis of Hexoctahedral Au−Pd Alloy Nanocrystals with High-Index Facets. *J. Am. Chem. Soc.* **2011**, *133*, 17114−17117.
(51) Nutariya, J.; Fayette, M.; Dimitrov, N.; Vasiljevic, N. Growth of Pt by Surface Limited Redox Replacement of Under Potentially Deposited Hydrogen. *Electrochim. Acta* **2013**, *112*, 813−823.
(52) Anjos, D. M.; Rigsby, M. A.; Wieckowski, A. Underpotential Deposition of Copper and Silver on Single Crystal Surfaces of Rhodium. *J. Electroanal. Chem.* **2010**, *639* (1−2), 8−14.
(53) Huang, X.; Zheng, N. One-Pot, High-Yield Synthesis of 5-Fold Twinned Pd Nanowires and Nanorods. *J. Am. Chem. Soc.* **2009**, *131* (13), 4602−4603.
(54) van der Vliet, D. F.; Wang, C.; Li, D.; Paulikas, A. P.; Greeley, J.; Rankin, R. B.; Strmcnik, D.; Tripkovic, D.; Markovic, N. M.; Stamenkovic, V. R. Unique Electrochemical Adsorption Properties of Pt-Skin Surfaces. *Angew. Chem., Int. Ed.* **2012**, *51* (13), 3139−3142.
(55) Dubau, L.; Maillard, F.; Chatenet, M.; André, J.; Rossinot, E. Nanoscale Compositional Changes and Modification of the Surface Reactivity of Pt_3Co/C Nanoparticles During Proton-Exchange Membrane Fuel Cell Operation. *Electrochim. Acta* **2010**, *56* (2), 776−783.
(56) Chen, Y.-H.; Hung, H.-H.; Huang, M. H. Seed-Mediated Synthesis of Palladium Nanorods and Branched Nanocrystals and Their Use as Recyclable Suzuki Coupling Reaction Catalysts. *J. Am. Chem. Soc.* **2009**, *131* (25), 9114−9121.
(57) Wang, L.; Nemoto, Y.; Yamauchi, Y. Direct Synthesis of Spatially-Controlled Pt-on-Pd Bimetallic Nanodendrites with Superior Electrocatalytic Activity. *J. Am. Chem. Soc.* **2011**, *133*, 9674−9677.
(58) Mitchell, C.; Fayette, M.; Dimitrov, N. Homo- and Hetero-Epitaxial Deposition of Au by Surface Limited Redox Replacement of Pb Underpotentially Deposited Layer in One-Cell Configuration. *Electrochim. Acta* **2012**, *85*, 450−458.
(59) Zhang, J.; Vukmirovic, M. B.; Xu, Y.; Mavrikakis, M.; Adzic, R. R. Controlling the Catalytic Activity of Platinum-Monolayer Electrocatalysts for Oxygen Reduction with Different Substrates. *Angew. Chem., Int. Ed.* **2005**, *44*, 2132−2135.
(60) Wang, L.; Yamauchi, Y. Metallic Nanocages: Synthesis of Bimetallic Pt−Pd Hollow Nanoparticles with Dendritic Shells by Selective Chemical Etching. *J. Am. Chem. Soc.* **2013**, *135* (45), 16762−16765.
(61) Yamamoto, K.; Imaoka, T.; Chun, W.-J.; Enoki, O.; Katoh, H.; Takenaga, M.; Sonoi, A. Size-Specific Catalytic Activity of Platinum Clusters Enhances Oxygen Reduction Reactions. *Nat. Chem.* **2009**, *1* (5), 397−402.
(62) Tang, L.; Han, B.; Persson, K.; Friesen, C.; He, T.; Sieradzki, K.; Ceder, G. Electrochemical Stability of Nanometer-Scale Pt Particles in Acidic Environments. *J. Am. Chem. Soc.* **2010**, *132* (2), 596−600.
(63) Dubau, L.; Lopez-Haro, M.; Durst, J.; Guetaz, L.; Bayle-Guillemaud, P.; Chatenet, M.; Maillard, F. Beyond Conventional Electrocatalysts: Hollow Nanoparticles for Improved and Sustainable Oxygen Reduction Reaction Activity. *J. Mater. Chem. A* **2014**, *2* (43), 18497−18507.
(64) Li, D.; Wang, C.; Strmcnik, D. S.; Tripkovic, D. V.; Sun, X.; Kang, Y.; Chi, M.; Snyder, J. D.; van der Vliet, D.; Tsai, Y.; Stamenkovic, V. R.; Sun, S.; Markovic, N. M. Functional Links between Pt Single Crystal Morphology and Nanoparticles with Different Size and Shape: The Oxygen Reduction Reaction Case. *Energy Environ. Sci.* **2014**, *7* (12), 4061−4069.

DOI: 10.1021/acsami.5b04021
ACS Appl. Mater. Interfaces 2015, 7, 17162−17170

(65) Shao, M.; Odell, J.; Humbert, M.; Yu, T.; Xia, Y. Electrocatalysis on Shape-Controlled Palladium Nanocrystals: Oxygen Reduction Reaction and Formic Acid Oxidation. *J. Phys. Chem. C* **2013**, *117* (8), 4172−4180.

DOI: 10.1021/acsami.5b04021
ACS Appl. Mater. Interfaces 2015, 7, 17162−17170